Available online at www.sciencedirect.com
ScienceDirect
Thermochimica Acta 465 (2007) 6–17
thermochimica acta
www.elsevier.com/locate/tca

Characterization and thermal degradation mechanism of isotactic polypropylene/carbon black nanocomposites

K. Chrissafis [a], K.M. Paraskevopoulos [a], S.Y. Stavrev [b], A. Docoslis [c], A. Vassiliou [d], D.N. Bikiaris [d,*]

[a] *Department of Solid State Physics, School of Physics, Aristotle University of Thessaloniki, GR-541 24 Thessaloniki, Macedonia, Greece*
[b] *Bulgarian Academy of Sciences, Space Research Institute, Department of Space Materials and Nanotechnologies, 6 Moskovska Street, Sofia, Bulgaria*
[c] *Department of Chemical Engineering, Queen's University at Kingston, Kingston, Ont., Canada K7L 3N6*
[d] *Laboratory of Organic Chemical Technology, Department of Chemistry, Aristotle University of Thessaloniki, GR-541 24 Thessaloniki, Macedonia, Greece*

Received 25 July 2007; received in revised form 20 August 2007; accepted 22 August 2007
Available online 4 September 2007

Abstract

Nanocomposites of isotactic polypropylene (iPP) and carbon nanoparticles (CN) were prepared using a twin-screw co-rotating extruder. Morphological characterization of the prepared materials was carried out by TEM and confocal micro-Raman. Viscoelastic and thermal properties were also determined by DMA and DSC measurements. Storage modulus was improved while the T_g was slightly increased. A small increase of melting temperature was obtained while crystallization temperatures were slightly altered. Degradation kinetics was investigated by thermogravimetric analysis (TGA and DTG). The nanoparticles' presence caused a shift of the onset mass loss temperature to higher temperatures. The activation energies were calculated using the isoconversional methods of Ozawa, Flynn and Wall (OFW) and Friedman and were found to be significantly enhanced by the presence of carbon black nanoparticles. Degradation took place in two autocatalysis stages, the first corresponding to a small initial mass loss, while the second, where substantial mass loss took place, was attributed to the main decomposition mechanism.

Keywords: Polypropylene; Carbon nanoparticles; Nanocomposites; Thermal degradation; Thermogravimetric analysis

1. Introduction

Various articles have been published on the thermal degradation of isotactic polypropylene (iPP) [1–17]. This is because the resource recovery of plastic wastes has significantly increased in importance and iPP is a major component of plastic wastes. Although its degradation is similar to that of polyethylene, the presence of the methyl groups of side chains results in intramolecular hydrogen transfer being more preferable in its degradation [1]. Thermogravimetric analysis (TGA) is a common method used to study kinetics of polymer degradations. This analysis can effectively assist in the determination of the degradation mechanisms, as well as predict the thermal stability of the polymers.

The following products of thermal degradation under vacuum of isotactic polypropylene were found with mass spectrometry: C_2H_4, C_3H_6, C_4H_{10}, C_4H_8, pentene, etc. [2]. The activation energy was shown to be 230.2 kJ/mol. Kiang et al. [3] using a first-order reaction model, under He atmosphere, obtained for E the value of 213.5 kJ/mol. Stuetz et al. [4] used isothermal thermogravimetric measurements to estimate an activation energy of 242.8 kJ/mol under N_2 atmosphere. First-order degradation kinetics was assumed to apply. Dickens [5] used factor-jump thermogravimetry. In vacuum, the apparent activation energy was estimated at 257.4 kJ/mol and in N_2 atmosphere it was 230.6 kJ/mol. De Amorim et al. [6] used both isothermal and non-isothermal measurements under He atmosphere. The values of E from non-isothermal measurements were between 220 and 300 kJ/mol, depending on the calculation method, and 280 kJ/mol from isothermal measurements. Szekely et al. [7] studied the degradation under Ar and He atmospheres at a low heating rate of 4 °C/min. He found that the maximum of the derivative mass loss (DTG) plot depends on the sample's mass

* Corresponding author. Tel.: +30 2310 997812; fax: +30 2310 997769.
E-mail address: dbic@chem.auth.gr (D.N. Bikiaris).

0040-6031/$ – see front matter © 2007 Elsevier B.V. All rights reserved.
doi:10.1016/j.tca.2007.08.007

and gas atmosphere. Day et al. [8], using different heating rates (0.5–10 °C/min) under N_2, determined the dependence of E on a with the Ozawa method, with E increasing monotonously with a between 130 and 200 kJ/mol. A kinetic model for the thermal degradation of polypropylene was developed by Chan and Balke [9] and fitted to molecular weight distribution data obtained by high-temperature size-exclusion chromatography. Using Arrhenius plots at constant reaction rates the average value of E was 123.8 ± 10.2 kJ/mol. Chan and Balke [10] also used thermogravimetric measurements under Ar atmosphere. Using Friedman's and Kissinger's methods they obtained data for the dependence of E on a. According to these two methods E increases monotonically from 90 to 190 kJ/mol. Values of E between 160 and 297 kJ/mol were also calculated with the Freeman–Carroll method. Applying a pseudo first-order reaction using two consecutive mechanisms the values for E for each heating rate separately were obtained. The calculated values of E were between 94.7 and 100.1 kJ/mol for the first mechanism and between 318.4 and 335.1 kJ/mol for the second one. Albano and de Freitas [11] showed that using the methods of Horowitz–Metzger, Van-Krevelen, Coats–Redfern and Freeman–Carroll the values of E vary between 121 and 259 kJ/mol. Bockhorn et al. [12] used a gradient free reactor with on-line mass spectrometry under isothermal conditions and an apparent activation energy of 220 kJ/mol was obtained. Wielage et al. [13] obtained the value of 273 kJ/mol for E using first-order reaction and the ASTM-E698 method. Gersten et al. [14] obtained for the apparent activation energy a value around 250 kJ/mol. Yang et al. [15] used a new method, the DTG curve fitting method, and obtained a value of 126 kJ/mol for E. Gao et al. [16] showed that a first-order reaction model cannot be applied to describe the thermal degradation of polypropylene. The appropriate reaction order was determined to be 0.35. They obtained under dynamic conditions values for E in the area of 129–139 kJ/mol for different heating rates and the value of 129 kJ/mol under isothermal degradation. Kumar and Madras [17] obtained a value of 134 kJ/mol for E using the Friedman method. Peterson et al. [18] show that the activation energy for degradation of PP has an initial value of about 150 kJ/mol at $\alpha = 0.05$ and increase to a maximum of 250 kJ/mol at $\alpha = 0.9$ under nitrogen, while it remains nearly constant at about 85 kJ/mol during the first 40% of degradation and steadily increases thereafter to a maximum of 270 kJ/mol at $\alpha = 0.9$ under air atmosphere.

It becomes obvious that the reported values are not consistent. These variations can be attributed to the different carrier gases used, such as Ar, He and N_2. Furthermore, difference in sample masses used under the same heating conditions has a similar effect. The different values of activation energy may also be the result of the different methods of calculation used and, also, the assumptions made before the calculation of E, such as that mass loss must be described as a single reaction step and the use of a first-order reaction mechanism.

The application of nanoparticles as fillers in polymeric nanocomposites has become appreciated in many commercial and scientific areas, with many studies having already been published on this subject [19–32]. The extraordinary properties of these materials are unprecedented for conventional microcomposites. Various synergisms between the properties of the two constituents lead to remarkable improvement of their properties, such as mechanical, electrical, gas permeability and thermal properties. Furthermore, the improvement is observed at very low filler loading (≤5 wt%). Since the large interfacial area formed is responsible for this behaviour, it is of the utmost importance that the filler is fully dispersed throughout the matrix.

The degradation process of nanocomposites has recently been described with the use of several kinetic models [33,34]. The presence of the nanofiller influenced the mechanism of degradation of the organic phase. In this study, iPP/CN nanocomposites, using carbon nanoparticles synthesized by a relatively new method, were prepared and characterized by TEM, DMA and DSC measurements. Thermogravimetry (TG) and differential thermogravimetry (DTG) measurements were performed and the thermal degradation kinetics of the nanocomposites prepared were studied and analyzed using various kinetic methods.

1.1. Kinetic methods for thermogravimetric analysis

For the kinetic studies the mass–temperature relation, which can predict the behaviour of the degradation reactions, must be examined. The purpose of these studies is to evaluate the kinetic parameters throughout the course of degradation, which, furthermore, allows an understanding of the decomposition mechanisms and of the relationship of the data obtained in the process with other interesting properties.

In kinetic studies of decomposition, the concentrations of the reactants and products are one of the main factors. When we combine the reaction rate and the Arrhenius expression, for non-isothermal measurements at constant heating rate $\beta = \mathrm{d}T/\mathrm{d}t$, we get the following basic expression:

$$\beta \frac{\mathrm{d}\alpha}{\mathrm{d}T} = A \exp\left(-\frac{E}{RT}\right) f(\alpha) \tag{1}$$

where T is the absolute temperature, $\mathrm{d}\alpha/\mathrm{d}T$ the reaction rate (t^{-1}), $f(\alpha)$ the function of the conversion depending on the mechanism of the degradation reaction, α being the degree of conversion of the mass loss, A the pre-exponential factor, E the activation energy (kJ/mol), and R is the gas constant.

The activation energy E can be calculated using various methods. One such is the isoconversional method of Ozawa, Flynn and Wall (OFW) [35–37], which is in fact a "model free" method which assumes that the conversion function $f(\alpha)$ does not change with the variation of the heating rate for all values of degree of conversion α. It involves measuring the temperatures corresponding to fixed values of α from experiments at different heating rates β. Therefore, plotting $\ln(\beta)$ against $1/T$ in the form of

$$\ln(\beta) = \ln\left[\frac{Af(\alpha)}{\mathrm{d}\alpha/\mathrm{d}T}\right] - \frac{E}{RT} \tag{2}$$

should give a straight line whose slope is directly proportional to the activation energy ($-E/R$).

Another method used is an isoconversional one. Friedman [38,39] proposed the use of the logarithm of the conversion rate

$d\alpha/dt$ as a function of the reciprocal temperature, in the form of

$$\ln\left(\frac{d\alpha}{dT}\right) = \ln\left(\frac{A}{\beta}\right) + \ln f(\alpha) - \frac{E}{RT} \quad (3)$$

It is obvious from Eq. (2) that if the function $f(\alpha)$ is constant for a particular value of α, then the sum $\ln f(\alpha) + \ln(A/\beta)$ is also constant. By plotting $\ln(d\alpha/dT)$ against $1/T$, the value of the $-E/R$ for a given value of α can be directly obtained. Using this equation, it is possible to obtain values for E over a wide range of conversions.

2. Experimental

2.1. Materials

The carbon nanoparticles (CN) used in this study were synthesized by a shock wave propagation method from the free carbon of the explosive [40]. Using optimal synthesis conditions (pressure, time, and temperature), carbon nanoparticles with controlled size and content were obtained. These consisted of disordered graphite (67 wt%) and diamond (33 wt%), as was characterized by X-ray diffraction analysis and had a mean diameter of 1–3 nm (TEM micrographs), a specific surface of 590 m^2/g and a specific gravity of 1.86 g/cm^3. Isotactic polypropylene was supplied by Basell Polyolefines and had a melt flow index (MFI) of 12 g/10 min at 190 °C, T_m = 162.1 °C and a degree of crystallinity 62.8%.

2.2. Preparation of nanocomposites

Nanocomposites containing 0.5, 1, 2.5 and 5 wt% CN were prepared by melt mixing in a Brabender (model *DSC Φ25/32D*) twin-screw co-rotating extruder with L/D 32 (D25 mm). Along the screw different screw elements existed which induced polymer melting and achieved fine dispersion of the nanoparticles in the polymer melt. The mixing section, after the nanoparticles' intake, enhanced the compounding and also increased the residence time of the mixture in the barrel. Barrel pressure at this part, as well as at the metering section before the die, were measured. The apparatus also included a vacuum vending port to remove any moisture traces or other volatile products formed during compounding.

Prior to the melt processing, the CN nanoparticles were dried for 24 h at 140 °C. The iPP pellets were fed into the throat of the extruder, while CN nanoparticles were introduced separately through a streamside feeding port further down the barrel directly into the polymer melt. Changing the feeding rate of each dosing unit automatically controlled the required proportions of both materials. Compounding was carried out using a screw rotating speed of 225 rpm and a temperature profile of 175, 180, 185, 190, 190, 195, and 190 °C at the sequential heating zones, from the hopper to the die. The melt temperature was continuously recorded during compounding. After compounding the material was extruded from a die, which had three cylindrical nozzles of 4 mm diameter, to produce cylindrical extrudates. These were immediately immersed in a cold-water bath (20 °C) and pelletized with an adjustable rotating knife located after the water bath, into 5 mm pellets.

2.3. Characterization of nanocomposites

2.3.1. Transmission electron microscopy

Electron diffraction (ED) and transmission electron microscopy (TEM) observations were made on ultra thin film samples of the various nanocomposites prepared by an ultramicrotome. These thin films were deposited on copper grids. ED patterns and TEM micrographs were obtained using a JEOL 120 CX microscope operating at 120 kV.

2.3.2. Micro-Raman spectroscopy

Raman studies of the iPP/CN samples were performed using a HORIBA/Jobin Yvon confocal micro-Raman spectrometer (Model: LadRAM), equipped with a 632 nm He/Ne laser source, 1800 1/nm grating and an Olympus BX41 microscope system. Collection of the spectra was performed at room temperature under the following conditions: 100× microscope objective, 100 μm pinhole size, 300 μm slit width, and 20 s exposure time. Each spectrum represents the average of two measurements. Sample profiling (2D mapping) was performed under the same conditions at a step increment of 0.5 μm in both *x*- and *y*-direction.

2.3.3. Dynamic thermomechanical analysis (DMA)

The dynamic thermomechanical properties of the nanocomposites were measured with a Perkin-Elmer Diamond DMA. The bending method was used at a frequency of 1 Hz in a temperature range of −50 °C to 155 °C. The heating rate was 3 °C/min. Testing was performed on rectangular bars measuring approximately 30 mm × 10 mm × 3 mm. These were prepared with a hydraulic press, at a temperature of 200 °C and a pressure of 100 bar, for a time period of 5 min. The exact dimensions of each sample were measured prior to measuring.

2.3.4. Differential scanning calorimetry (DSC)

A Perkin-Elmer Pyris 1 differential scanning calorimeter (DSC), calibrated with Indium and Zinc standards, was used. Samples of 5 ± 0.1 mg were used in the tests. They were sealed in aluminum pans and heated up to 200 °C at a rate of 10 °C/min to record the melting behaviour. The samples were held at that temperature for 5 min in order to erase any thermal history. Non-isothermal crystallization measurements were then carried out at a cooling rate of 10 °C/min down to 25 °C. All measurements were repeated at least two times.

2.3.5. Thermogravimetric analysis

Thermogravimetric analysis was carried out with a SETARAM SETSYS 1750 TG/DTA. Samples (11 ± 0.5 mg) were placed in alumina crucibles. An empty alumina crucible was used as reference. Samples were heated from ambient temperature to 500 °C in a 50 ml/min flow of N_2. Heating rates of 5, 10, 15 and 20 °C/min were used and continuous recordings of the heat flow, sample temperature, sample weight and its time

derivative were taken. All measurements were repeated at least three times.

3. Results and discussion

3.1. Morphological characterization

Due to the nature of their preparation, the carbon black nanoparticles were found to contain surface hydroxyl groups, as revealed by the characteristic broad peak at 3300–3700 cm^{-1} obtained through FTIR spectroscopy (data not shown). It seems that the formation of these groups cannot be avoided during their preparation. A much earlier study by Rivin showed that carbon black nanoparticles exhibit on their surface about 3 –OH and 0.05 –COOH groups per nm^2 [41]. CN is finely dispersed in the iPP matrix at low loadings (up to 1 wt%) (Fig. 1). However, at 2.5 and 5 wt% loadings there is a tendency for agglomeration. This behaviour should be attributed to the existence of the above-mentioned reactive groups, which have the ability to form hydrogen bonds between them. As found from our previous study, these agglomerates caused a slight decrease of tensile strength and elongation at break, whereas Young's modulus and tensile strength at the yield point were substantially improved [42]. The agglomerates were visualized by TEM micrographs (Fig. 1) where nanoparticles in the range of 200–1000 nm are observed, as well as with confocal micro-Raman spectroscopy (Fig. 2), which revealed a fair distribution of the nanoparticles in the polymeric matrix.

Micro-Raman spectroscopy also was used in previous studies of polypropylene composites [43] as well as on its nanocomposites to detect the thermal residual strains and chain orientation [44–46]. Here, visualization of the agglomerates inside the polymer matrix was performed through the two-dimensional (XY) spatial profiles of the Raman band at 1594 cm^{-1}, acquired from randomly selected areas of the composites. Previous Raman examination of this CN [42] showed the presence of a broad band having a maximum intensity at 1594 cm^{-1}, resulting from the combination of peaks at 1582 cm^{-1} ("G-band", in-plane displacement of carbon atoms strongly coupled to hexagonal graphite sheets) and 1620 cm^{-1} (presence of significant disorder in the graphite lattice). Fig. 2 shows characteristic 2D profiles corresponding to iPP/CN composites of 0.25 and 2.5 wt%, respectively. The yellow and red areas (high signal intensity) indicate the presence of CN agglomerates, whereas dark blue represent areas in the composite devoid of CN aggregates. Areas of intermediate color (light green and blue) are taken as representative of parts in the film where CN is present in fine dispersion ($\leq$500 nm) within the iPP matrix.

The results show that composites of low CN content (0.25 wt%; Fig. 2a) exist in relatively homogeneous dispersion and contain only small agglomerates with size approximately equal to 1 μm or less. Higher CN contents (2.5 wt%; Fig. 2b) result in the formation of larger agglomerates with sizes varying between 1 and 5 μm. Raman spectra acquired from composites with CN concentrations in the range 0.5–5 wt% (not shown here) also reveal a trend of increasing aggregate size with concentration. However, it should be pointed out that higher concentrations do not result exclusively in the formation of large CN agglomerates. As seen in Fig. 2, smaller aggregates and areas of fine particle dispersion can still be observed. The trend of CN agglomerate coarsening with concentration can offer a possible explanation for the reduced mechanical properties – tensile strength and elongation at break – exhibited by the nanocomposites with higher filler loadings: larger agglomerates can act as points of mechanical failure inside a polymer matrix, thus reducing the overall mechanical properties of the composite.

3.2. Viscoelastic and thermal properties of the prepared materials

Dynamic thermomechanical analysis (Fig. 3) verified that carbon black nanoparticles impart a toughening effect on the polymer. When added to polymer matrices, nanoparticles are known to cause a considerable change in the dynamic properties of the pristine material. Since storage modulus (G') is mainly related to the structure network created between the nanoparticles and macromolecular chains a considerable increase should be recorded. Wang reported [47] that due to polymer-filler inter-

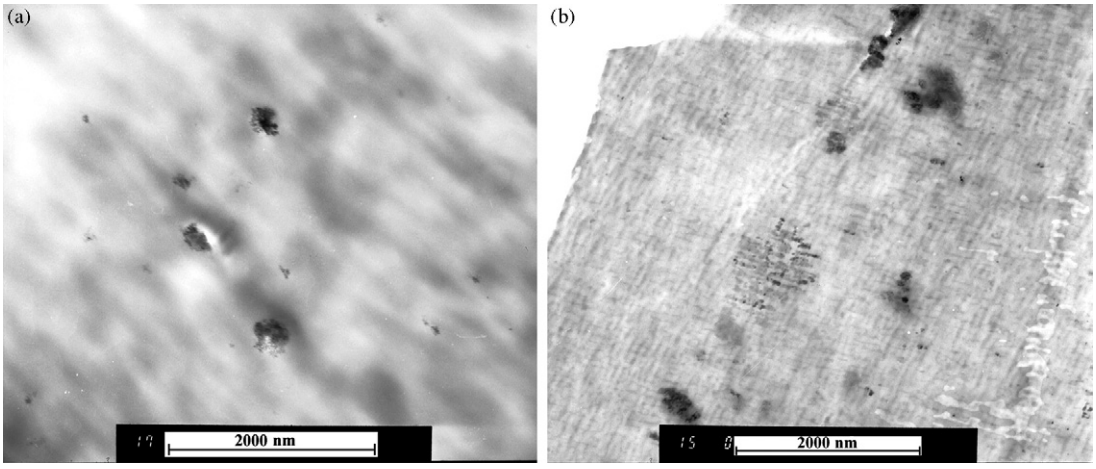

Fig. 1. TEM micrographs of the iPP/CN nanocomposites containing (a) 0.25 wt% and (b) 1 wt% CB nanoparticles.

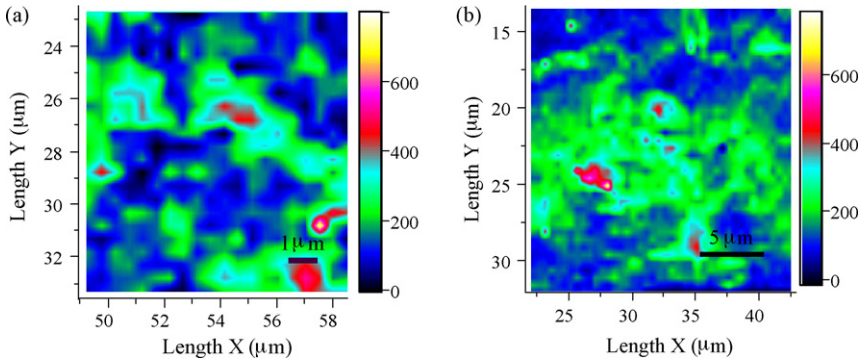

Fig. 2. Micro-Raman 2D maps from samples containing (a) 0.25 wt% and (b) 2.5 wt% CN, respectively. The colour bar indicates peak intensity at 1594 cm^{-1}.

actions the adsorption of the polymer chains on the filler's surface reduces the mobility of the polymeric segments. This transition zone surrounding the nanoparticles has a higher modulus and T_g, both of which are gradually reduced as the distance from the filler surface is increased. Furthermore, when the filler–filler interactions are more favourable than those between the filler and the matrix, the nanoparticles tend to form agglomerates. The polymer entrapped into these agglomerates also exhibits a higher modulus than the neat polymer. In the prepared nanocomposites, as seen in Fig. 3a, the storage modulus at low temperatures is indeed increased by increasing the CN content. However, this increase is less obvious at higher temperatures, since the mobility of the iPP macromolecules is very high above the glass transition temperature.

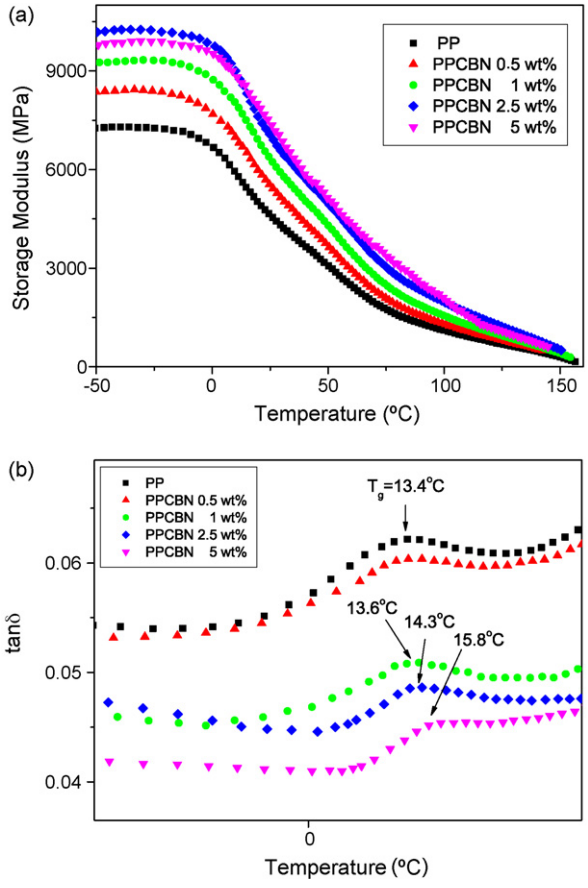

Fig. 3. Dynamic mechanical relaxation behaviour of iPP/CN nanocomposites containing different CN content: (a) storage modulus (E') and (b) tan δ.

Examining the tan δ variation curves, two relaxations are observed, identified as α and β, in order of decreasing temperature. The α-relaxation recorded at 80–100 °C is usually related to the crystalline–amorphous polymer regions and the softening point of iPP while the β-relaxation recorded at −5 °C up to 40 °C is attributed the T_g of iPP (Fig. 3b). According to these curves neat iPP exhibits a T_g at 13.4 °C. Almost identical T_g*s* are also obtained for the nanocomposites containing CN up to a concentration of 1 wt%. Usually, the T_g of a polymer matrix tends to increase with the addition of nanoparticles, due to the interactions between the polymeric chains and the reduction of the macromolecular chain's mobility at the interface around the nanoparticles. However, reports in the literature can be found, whereat it is reported that the T_g either remains unaffected by the addition of inorganic nanoparticles [21,48,49], increases [50,51], or even decreases [52]. So it seems that this effect is not consistent, but depends on the microstructure/amount of the nanoparticles, as well as the interactions taking place between the polymer and filler [53]. In the prepared iPP/CN nanocomposites, by increasing the amount of CN up to 2.5 and 5 wt%, a slight shift of the recorded T_g is observed (14.3 and 15.8 °C, respectively; Fig. 3b). This is probably related to the interactions between iPP/CN and, most likely, to the agglomerates formed by the carbon nanoparticles, due to the presence of reactive groups on their surface.

In Fig. 4a the DSC thermograms of iPP and its nanocomposites with different CN amounts are presented. iPP has a melting temperature of 163 °C, while in almost all nanocomposites there is a clear shift of this temperature to higher values. There is an increase up to 168 °C for nanocomposites containing 0.5 and 1 wt% CN, while for higher CN loadings, 2.5 and 5 wt%, it is slightly reduced to 166 and 164 °C, respectively. The melting point increase may be attributed to the crystallization effect of CN. As found from our previous study with polarized optical microscopy, CN can act as a nucleating agent increasing the rate of crystallites' formation and dramatically reducing the size of the formed crystallites to sizes lower than 1 μm [42]. A similar nucleating effect was also mentioned in iPP by fumed silica nanoparticles [54]. The melting point of polymer crystals is a function of the lamellar thickness and the degree of perfection. Consequently, this increase of melting point should

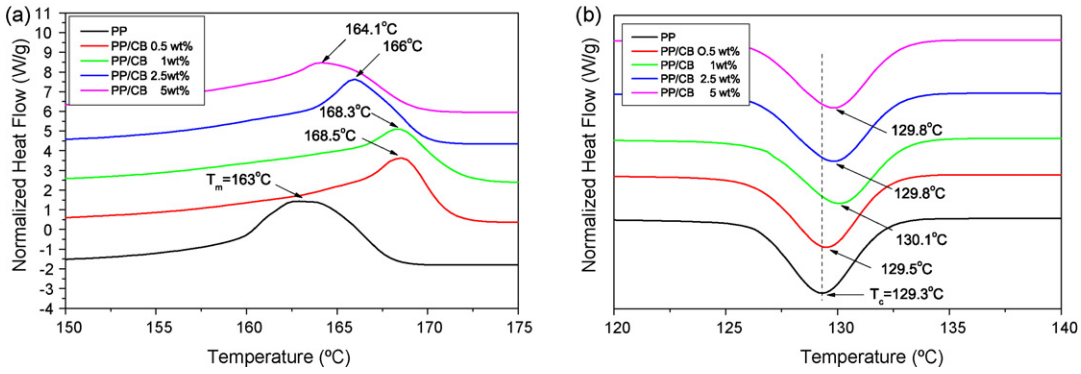

Fig. 4. DSC thermograms of iPP/CB nanocomposites during (a) heating and (b) cooling from the melt.

be attributed to the formation of crystals with narrower sizes and fewer defects, since crystallization remained stable or was increased by only 1–2% in nanocomposites with 1 and 2.5 wt% CB. The higher crystallization rates of iPP/CN were also verified by the crystallization temperatures recorded during cooling from the melt (Fig. 4b).

3.3. Thermal degradation kinetics

Thermal degradation of iPP and its nanocomposites with different concentrations of CN were studied by determining their mass loss during heating. In Fig. 5 the mass loss (TG%) and the derivative mass loss (DTG) curves of all studied samples are presented at a heating rate of 10 °C/min. During the thermal degradation it seems that all the samples showed a single step of degradation (Fig. 5a and b). Pure polypropylene begins to volatilize at about 273 °C, while the presence of carbon black causes a shift of the initial mass loss towards higher temperatures (about 315 °C for iPP/5 wt% CN). There is a clear shift of initial decomposition temperature of almost 40 °C at higher temperatures. From the thermogravimetric curves it can be seen also that iPP and the samples with different concentration of carbon black present a relative good thermostability, since no remarkable mass loss occurred until 335 °C (<0.5%). As seen from the peak of the first derivative, the temperature at which iPP decomposition rate is the highest is T_p = 452.3 °C, for a heating rate of 10 °C/min (Table 1) while a small shift to higher temperatures was observed with concentration of CN. CN enhances the thermal stability of the samples, as seen in Table 1, at the starting temperature of the degradation, the temperature corresponding to initial 2% of mass loss (T_d) and the peak temperature (T_p) of the DTG curve. Analogous behaviour, regarding the improvement of the thermal stability of iPP nanocomposites, in an inert atmosphere, has been reported in literature and is attributed to the shielding effect of nanoparticles inhibiting the elimination of the formed volatile by-products [55–57]. Pure isotactic polypropylene almost completely degrades while the residues in the nanocomposite samples with CN are almost consistent with the amount of the additive having been introduced in the polymer (Table 1).

The reaction mechanism of polymer decomposition is a very complex radical chain mechanism, including initiation reac-

Table 1
Characteristic thermal decomposition temperatures and remaining residue of iPP/CN nanocomposites

Sample	Onset (°C)	T_p (°C)[a]	T_{max}(°C)[b]	T_d (°C)	Residue%
iPP	273.6	452.3	451.8	368.0	0.2
iPP/1 wt% CN	280.8	454.3	452.1	375.3	0.7
iPP/2.5 wt% CN	285.4	455.6	452.0	394.6	1.9
iPP/5 wt% CN	315.6	462.8	459.8	418.6	4.8

[a] T_p: peak temperature of DTG curve.
[b] T_{max}: decomposition temperature of the DSC curve.

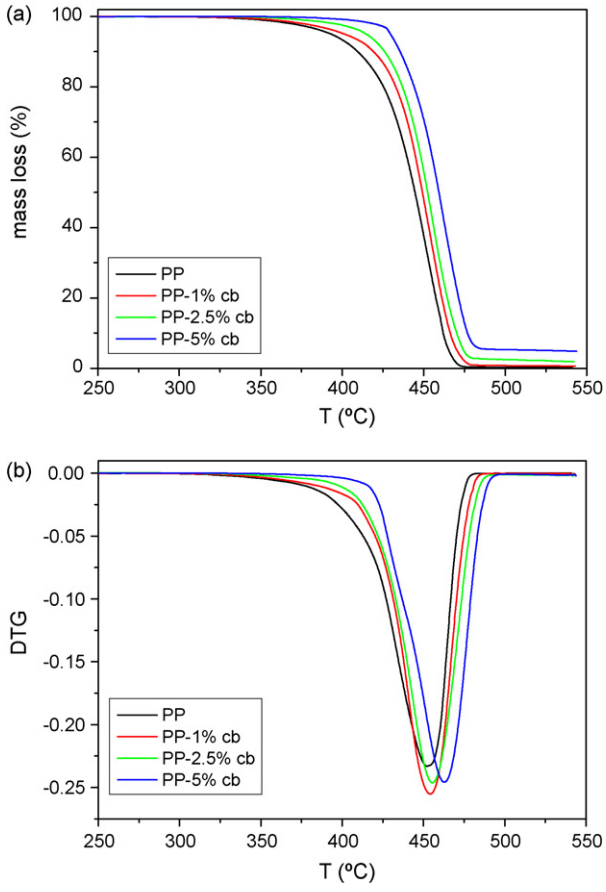

Fig. 5. (a) Mass loss (TG%) and (b) derivative mass loss (DTG) vs. temperature at a heating rate of β = 10 °C/min as a function of CN concentration in the sample.

tions, propagation reactions and termination reactions. Reports on the degradation products of iPP under different heating profiles and carrier gases can be found in the literature [1,2,58,59]. The activation energies presented at these studies cover a wide range of values from 120 kJ/mol up to 300 kJ/mol. These variations could be attributed to the different carrier gases used, such as Ar, He and N_2. According to Szekely et al. [7] using either Ar or He the peak temperature of the DTG curve for the same sample differs significantly (∼12 °C for a heating rate of 4 °C/min and a mass of 3 mg). Difference in sample masses used under the same heating conditions has a similar effect (∼13 °C for a heating rate of 4 °C/min and sample masses 0.35 and 3 mg) [7].

In order to more thoroughly analyze the degradation mechanism of iPP and the effect of the different concentrations of CN it is important that the kinetic parameters (activation energy E and pre-exponential factor A) and the conversion function $f(\alpha)$ be evaluated. The relationship between kinetic parameters and conversion (α) can be found using the mass loss curves recorded in the TG dynamic thermograms. The degradation for all the samples was studied through non-isothermal measurements at different heating rates (5, 10, 15, and 20 °C/min). In Fig. 6 the mass loss at different heating rates for iPP and one of the samples containing CN are presented as examples. As can be seen, increasing the heating rate results in a shift of the degradation area to higher temperatures. The same is concluded for the rest of the samples.

As is well known, two main types of kinetic models are generally applied for thermal degradation of polymers: the *n*th-order model with only one parameter, the reaction order, and the first-order model. Other models have also been used occasionally but they are complex models containing several fitting parameters. Moreover, the calculation of the activation energy, is accomplished using only one heating scan or different heating rates, each separately. As noted earlier, these choices of methods have resulted in a very wide range of reported activation energy values. With the use of a suitable correlation program we examined these cases, with the direct, however, correlation between the experimental and theoretical values. The examination covered initially the pristine material, to the extent permitted by experimental data available in the open literature, subsequently, the obtained conclusions were tested on the materials containing the CN. In Fig. 7 indicative results of the correlation for one heating rate for pristine iPP using the first and *n*th-order models are presented. The results are similar for the other heating rates and for the samples containing CN. In Fig. 7a, it is deemed that the correlation is relatively satisfactory for the

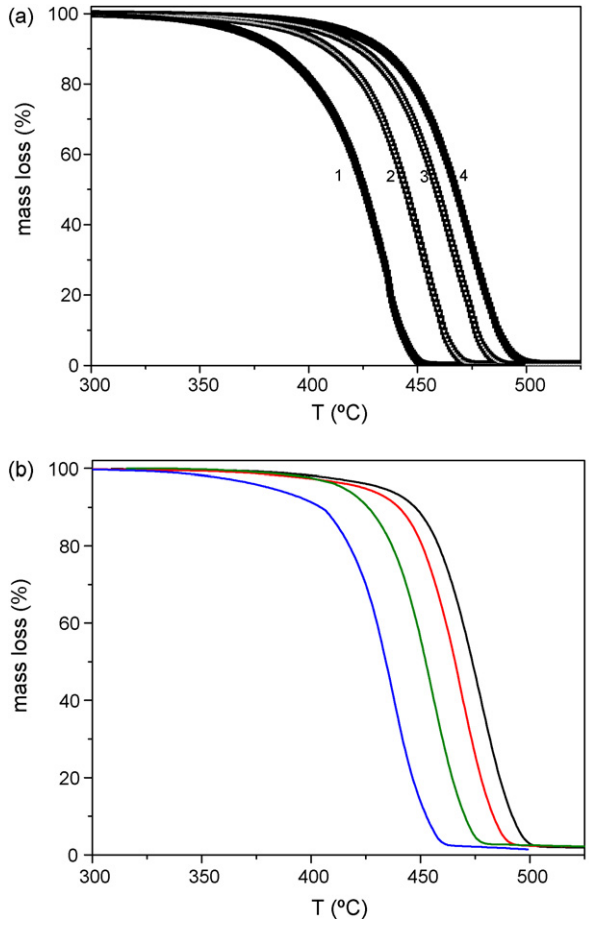

Fig. 6. Mass loss (TG%) curves of (a) iPP and (b) iPP/CN 2.5 wt% samples at different heating rates (1: $\beta = 5$ min/°C, 2: $\beta = 10$ min/°C, 3: $\beta = 15$ min/°C, 4: $\beta = 20$ min/°C).

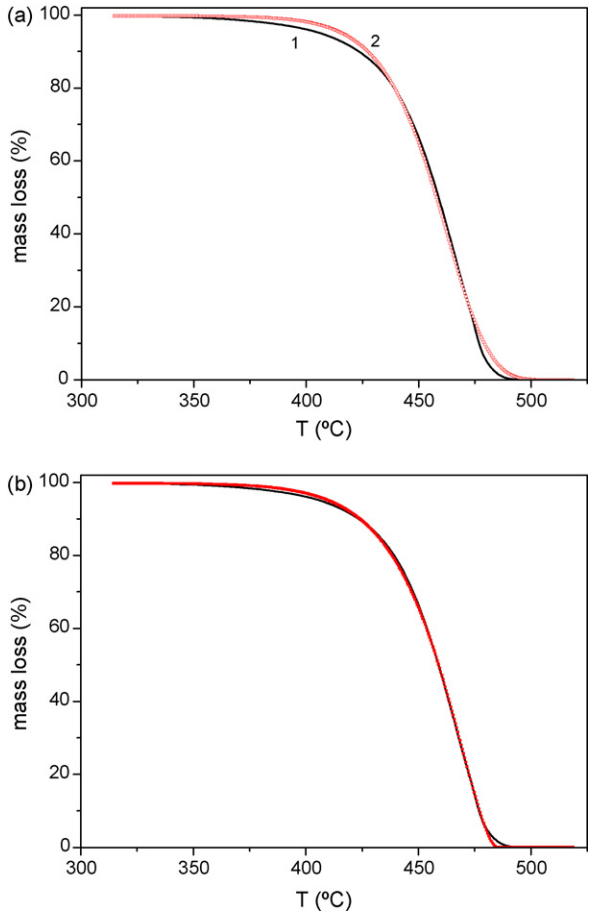

Fig. 7. Mass loss (TG%) curve of iPP sample at a heating rate of $\beta = 15$ °C/min and its fitting curve with (a) a first-order model and (b) a *n*th-order model (1: experimental curve, 2: fitting curve).

area of mass loss between 20 and 80 wt%, while it diverges noticeably at the two extreme areas. The activation energy calculated was 251.2 kJ/mol and the pre-exponential factor was $\log A = 15.9$.

In Fig. 7b the correlation is significantly improved for the middle area, as well as for the two ends of the curve. Nevertheless, the deviation is still considerable at the two extreme areas. Adopting a *n*th-order model not only changes the calculated order of the reaction, since *n* becomes 0.45, but the values of the other two kinetic parameters, *E* and *A*, are notably different. The values of the activation energy and the pre-exponential factor are reduced, from 251.2 to 197.4 kJ/mol for *E* and from 15.9 to 11.9 for $\log A$. From this example the strong dependence of E from the adopted model used for its calculation through such a procedure can be seen. Furthermore, it is of particular importance that the correlation using experimental results from one heating rate each time results in different calculated values of activation energy and pre-exponential factor for the same material. This variation is particularly large for the pre-exponential factor. For this reason the results of kinetic analysis of any material are more reliable when at least three different heating rates are used simultaneously for the correlation. Having ascertained this, we examined the possibility of correlating the experimental and theoretical data using four different heating rates together with the first-order and *n*th-order model. The results of this correlation are presented in Fig. 8.

As can be seen in Fig. 8, the correlation with the help of the first-order model is unacceptable while significant improvement is observed when the *n*th-order model is used (Fig. 8b). However, despite this improvement, the correlation cannot be accepted. The resulting value of activation energy in this case is $E = 149.7$ kJ/mol and of pre-exponential factor $\log A = 8.4$, while *n* is equal to 0.3.

The correlation process for each heating rate separately or altogether, with the help of a first-order model and an *n*th-order model, does not lead to acceptable results and generates a wide range of calculated activation energy values. Gao et al. [16] arrived at similar conclusions regarding the use of a first-order model for each rate separately, suggesting in turn the use of an *n*th-order model with $n = 0.35$. The analysis leads to a narrow distribution of values for *E* and a wider for *A*, which must be associated with the limited range of heating rates used and the restriction of the correlation area from 10 to 90% mass loss. If, however, the mean values of *E* and *A* are used for the simultaneous correlation of the experimental results for all the heating rates used, they lead again to unacceptable results. Until today no theoretical explanation has been presented which substantiates that the basic kinetic parameters *E* and *A* depend in a different way on the heating rate, for the commonly used rates, which leads in not obtaining acceptable results by this process of correlation.

In polymer degradation the processes involved are usually chain reactions. That is, $f(\alpha)$ represents a series of elemental steps, with each step having its own kinetic parameters. Due to the complexity and the mass of the different stages it is very rarely is it attempted to describe the reaction with the help of multiple mechanisms. Chan [9,10] presents a kinetic model with

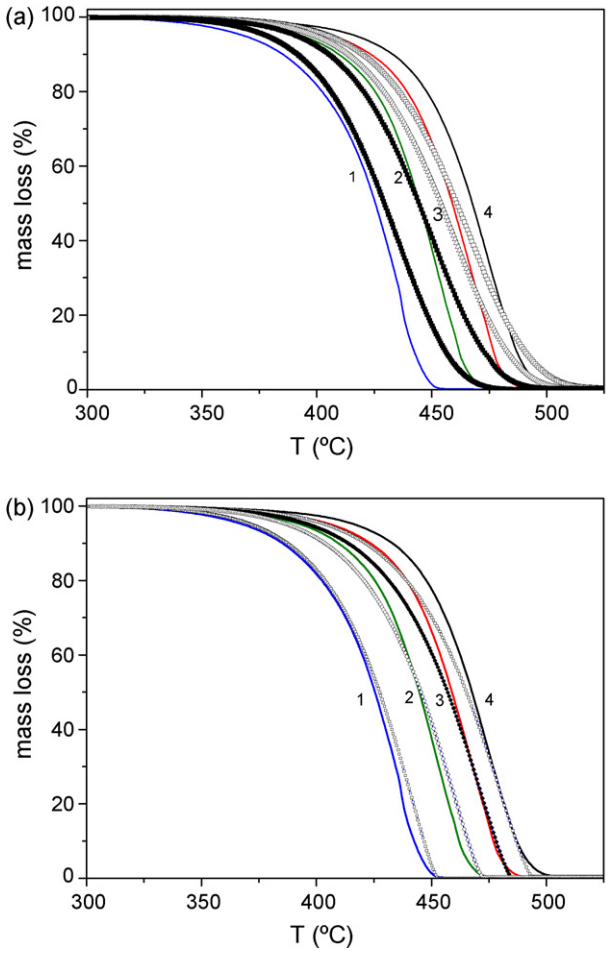

Fig. 8. Mass loss (TG%) curves of iPP samples at different heating rates β and their fitting curves with (a) a first-order model and (b) a *n*th-order model (1: $\beta = 5$ min/°C, 2: $\beta = 10$ min/°C, 3: $\beta = 15$ min/°C, 4: $\beta = 20$ min/°C).

two consecutive first-order reactions for each heating rate separately. In Fig. 9 the correlation results are presented for a heating rate of 15 °C/min with the help of two consecutive first-order reactions. As can be observed, the correlation is quite satisfactory. The values obtained are: for the first area $E = 172.2$ kJ/mol

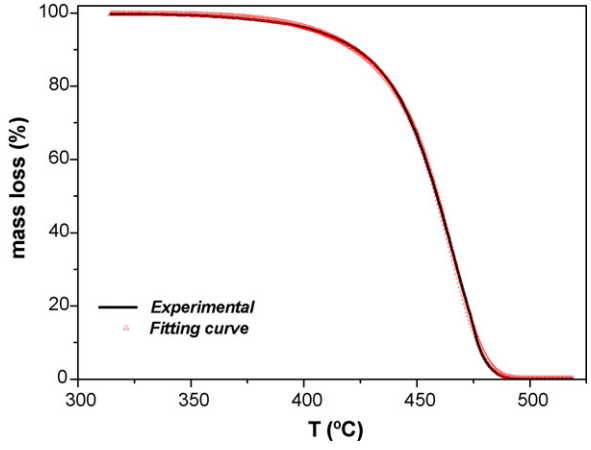

Fig. 9. Mass loss (TG%) curve of iPP sample with heating rate $\beta = 15$ °C/min and its fitting curve for two consecutive first-order reactions.

and $\log A = 10.6$ and for the second area $E = 313.1$ kJ/mol and $\log A = 20.4$. These results for the second area are similar to the results of Chan [9,10]. As in the case of correlation using a first-order model, assuming a one-step degradation, the values of the activation energy, but even more for A, present a very large variation (from 4.5×10^{22} to 1.4×10^{24}). If these values are used for the correlation of all the heating rates together the result is not at all acceptable.

From this analysis we can conclude that for correlation of the experimental results using the model of the first and nth-order so much for each heating rate separately as well as for all the rates together with the help of the two consecutive first-order reactions the results are not acceptable.

As we demonstrated in the previous analysis, the estimated values of activation energy for many of the methods used for its calculation which presuppose an initial model selection lead to great variations. Therefore, here we used methods of calculation which do not require knowledge of the kinetic equation a priori, at least for the estimation of E. For the calculation of the activation energies all heating rates were used and they were estimated using the Ozawa, Flynn and Wall (OFW) and Friedman methods for the sake of comparison. Firstly, the isoconversional Ozawa method was used to calculate the activation energy for different conversion values and the results are shown in Fig. 10a. Secondly, the Friedman method was used by plotting $\ln(d\alpha/dT)$ against $1/T$ for a constant α value and, thus, the activation energy was calculated (Fig. 10b).

The dependence of E on α value, as calculated with Friedman and Ozawa methods, presents almost the same tendency. Small variations are basically observed at the very initial and final stages, with the Friedman method being more sensitive in those areas. The difference in the E value calculated by the two methods can be explained by a systematic error due to improper integration. The method of Friedman employs instantaneous rate values being, therefore, very sensitive to experimental noise. In the Ozawa method, the equation used is derived assuming a constant activation energy, introducing systematic error in the estimation of E in the case that E varies with α, an error that can be estimated by comparison with the Friedman method results [60].

It is deduced from Fig. 10 that the dependence of E on α value can be separated in two distinct regions for iPP and iPP with 1% carbon black. The first one for values of α up to 0.2, in which E presents a rapid increase, and the second one ($0.2 < \alpha < 1$) in which E presents a slight increase, being almost stable. This dependence of E on α is an indication of a complex reaction with the participation of at least two different mechanisms, from which one has quite a small effect on mass loss. The "two mechanisms" – as a result of the increasing E with a – is a rather typical phenomenon for many polymers [18]. From the two mechanisms, the first corresponds to the part where small mass loss appears, while the second part, where the substantial mass loss takes place, is attributed to the main decomposition mechanism, each mechanism presenting different activation energy. The samples of iPP containing 2.5 and 5 wt% CN exhibit a much smaller value fluctuation and are more stable over the entire value area of a, as can be principally seen in Fig. 10a. This is expected to translate in the contribution of a second mechanism possibly being very small.

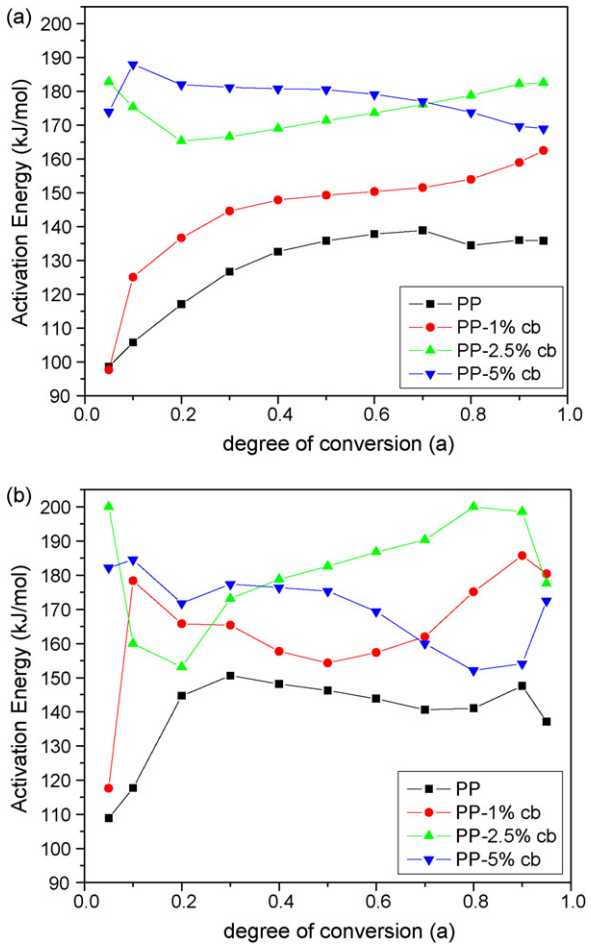

Fig. 10. Dependence of the activation energy (E) on the degree of conversion (α) of the mass loss, as calculated with (a) Ozawa's method and (b) Friedman's method for the different samples.

In order to determine the conversion function $f(\alpha)$ we used a method referred to as the "model fitting method" [61]. This method, that does not assume knowledge of E and $f(\alpha)$ in advance, was applied simultaneously on the experimental data taken at heating rates of $\beta = 5$, 10, 15 and 20 °C/min. It has been shown that the model-fitting method to multiple heating rates data gives activation energies similar to the values estimated by the isoconversional methods [62]. For the fitting of the mass loss experimental curve, 16 different kinetic models were used. For the determination of the nature of the mechanisms through the comparison of the experimental and theoretical data, initially it is considered that the degradation of the samples can be described only by a single mechanism that corresponds to the main mass loss, without presuming the exact mechanism. Having determined this mechanism ($f(\alpha)$), the data of the other mechanisms are determined, which correspond to the small mass loss part, hence a better correlation between experimental and theoretical data can be achieved. In Fig. 11 the results of the best fitting using one kinetic model can be seen for pristine iPP and iPP containing 5 wt% CN. The results for the other two samples are analogous.

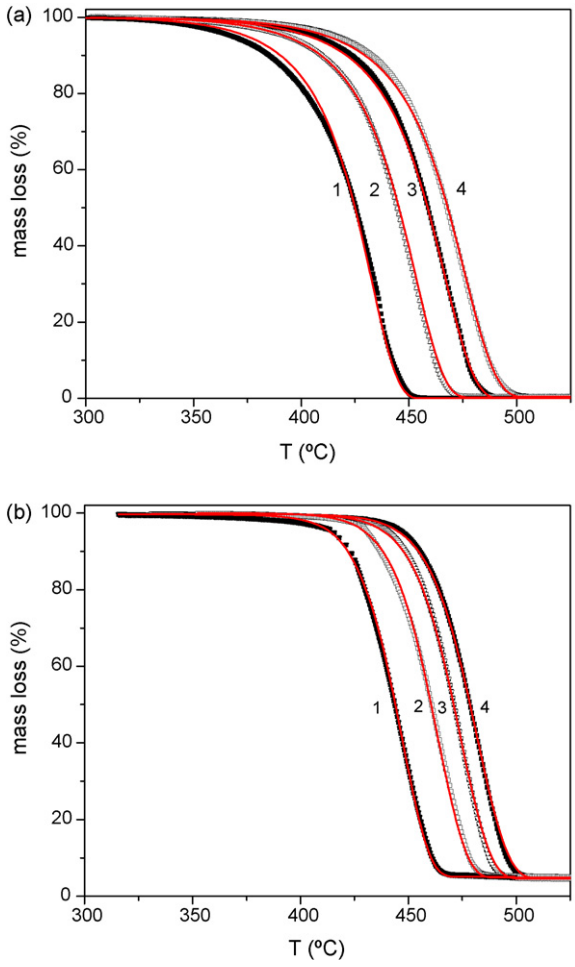

Fig. 11. Mass loss experimental data of (a) pure iPP and (b) iPP contining 5 wt% CN and fitting curves for different heating rates and for one reaction mechanism (1: $\beta = 5$ min/°C, 2: $\beta = 10$ min/°C, 3: $\beta = 15$ min/°C, 4: $\beta = 20$ min/°C).

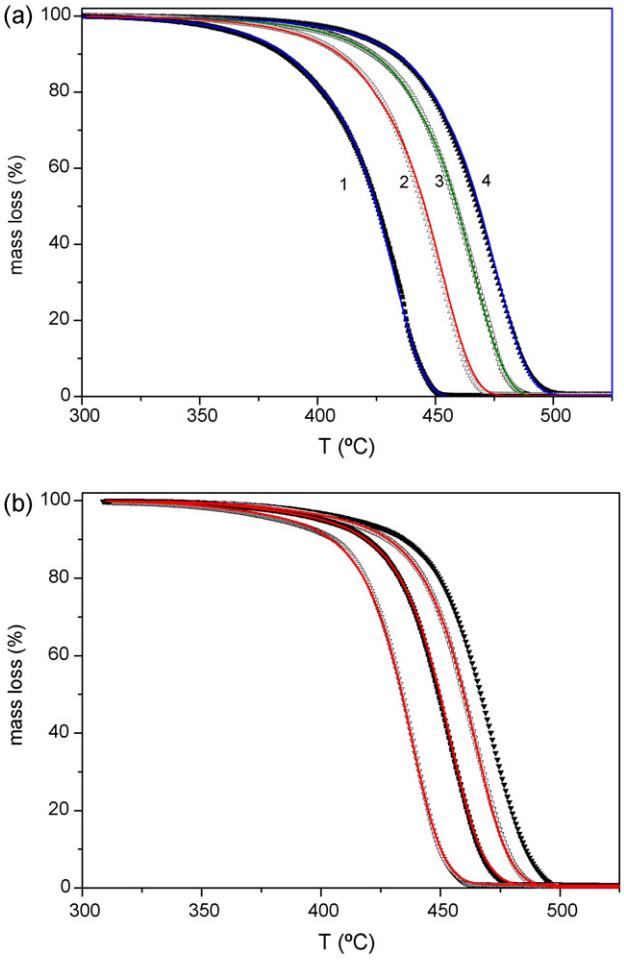

Fig. 12. Mass loss experimental data of (a) iPP and (b) iPP containing 1% CN and fitting curves for different heating rates and for two consecutives reactions mechanism.

The fitting with two different forms of the conversion function is acceptable, with the correlation factors being better than 0.9992. These forms are: the *n*th-order reaction with autocatalysis $f(\alpha) = (1-\alpha)^n(1 + K_{cat}X)$ and the expanded Prout–Tompkins equation (autocatalytic reaction) $f(\alpha) = (1-\alpha)^n\alpha^m$ [63]. As seen, the fitting to the experimental data is very good for almost the whole area, while there is a slight divergence for the region where the mass loss takes lower values. The correlation is better for the samples containing CN. The form of the conversion function, obtained by the best fitting, is the mechanism of autocatalysis *n*th-order, where K_{cat} is a constant and X the reactants for iPP and for all the samples containing CN. The calculated values for the activation energy E, the pre-exponential factor $\log A$ (s^{-1}), the reaction order n and the correlation coefficient are presented in Table 2.

The values of the activation energy are in the area of the calculated values from the Ozawa and Friedman methods. Exponent value n diverges considerably from the value 1, which is usually used for the kinetic description of mass loss in polymers [64–68], mainly for the sample iPP. Comparing the results of the fitting and the dependence of E on α, the possibility of improving the correlation with the help of a second mechanism is made clear.

For the determination of the first stage mechanism for iPP, as well as for the samples with carbon black, the following are assumed: (a) the two mechanisms are consecutive, and (b) this mechanism, which we try to identify, corresponds to a small mass loss, according to the experimental results. The fitting with two consecutive mechanisms leads to a remarkable improvement in the fitting of the experimental results with the theoretical ones (Fig. 12a). Similar are the results for the sample iPP containing 1 wt% CN (Fig. 12b). The correlation of the experimental results for samples iPP with 2.5 and 5 wt% CN with the use of two consecutive mechanisms did not yield any improvement.

Table 2
Activation energies, pre-exponential factors, reaction order and correlation coefficients of all samples after fitting with one reaction mechanism

Sample	E (kJ/mol)	$\log A$ (s^{-1})	Reaction order, n	Correlation coefficient
iPP	129.8	6.65	0.7	0.9995
iPP/1 wt% CN	145.5	7.51	1.0	0.9997
iPP/2.5 wt% CN	171.7	9.30	1.1	0.9997
iPP/5 wt% CN	174.7	10.00	0.9	0.9997

Table 3
Activation energies, pre-exponential factors, reaction orders and correlation coefficients of all samples after fitting with the two consecutive reaction mechanisms

Sample	First reaction mechanism ($0 < \alpha < 0.2$)			Second reaction mechanism ($\alpha > 0.2$)		
	E_1 (kJ/mol)	$\log A_1$ (s^{-1})	N_1	E_2 (kJ/mol)	$\log A_2$ (s^{-1})	n_2
iPP	92.7	4.5	0.15	139.5	7.5	0.79
iPP/1 wt% CN	96.9	4.9	0.15	159.9	8.8	1.09
iPP/2.5 wt% CN	–	–	–	171.9	9.3	1.10
iPP/5 wt% CN	–	–	–	174.7	10.0	0.90

The form of the conversion function, obtained by the best fitting, with a correlation factor better than 0.9999, is the mechanism of autocatalysis n-order $f(\alpha) = (1-\alpha)^n(1 + K_{cat}X)$, for all the studied samples. In this stage of identification, for the best possible results, we left the parameters (E, A and n) of the second mechanism to be recalculated. The theoretical data fits very well with the experimental data in the first area of small weight loss. The results from all the different samples are summarized in Table 3.

4. Conclusion

Nanocomposites of isotactic polypropylene (iPP) and carbon nanoparticles (CN), synthesized by a shock wave propagation method from the carbon of the explosive, were prepared using a twin-screw co-rotating extruder. Morphological characterization of the prepared materials was carried out by TEM and micro-Raman studies. At low loadings the filler was finely dispersed while at higher loadings there was a tendency for agglomeration. Viscoelastic and thermal properties were also determined by DMA and DSC measurements. Storage modulus was increased, especially at lower temperatures, while the T_g slightly shifted to higher temperatures. A small increase of the melting temperature was obtained, up to 5 °C, while crystallization temperatures were not significantly altered.

Degradation kinetics were extensively investigated by thermogravimetry analysis TGA and DTG. The presence of the nanoparticles caused a shift of the onset mass loss temperature to higher temperatures. The activation energies were calculated using the isoconversional methods of Ozawa, Flynn and Wall (OFW) and Friedman and were found to be significantly increased. Degradation took place in two autocatalysis stages, the first corresponding to a small initial mass loss, while the second, where substantial mass loss took place, was attributed to the main decomposition mechanism.

References

[1] R.P. Lattimer, J. Anal. Appl. Pyrol. 31 (1995) 203.
[2] V.D. Moiseev, M.B. Neiman, A.I. Kriukova, Polym. Sci. USSR 2 (1961) 55.
[3] J.K.Y. Kiang, P.C. Uden, J.C.W. Chien, Polym. Degrad. Stab. 2 (1980) 113.
[4] D.E. Stuetz, A.H. Diedwardio, F. Zitomer, B.P. Barnes, J. Polym. Sci. C 13 (1975) 585.
[5] B. Dickens, J. Polym. Sci. C 20 (1982) 1169.
[6] M.T.S.P. de Amorim, C. Bouster, J. Veron, J. Anal. Appl. Pyrol. 4 (1982) 103.
[7] T. Szekely, G. Varhegyi, F. Till, P. Szabo, E. Jakab, J. Anal. Appl. Pyrol. 11 (1987) 83.
[8] M. Day, J.D. Cooney, M. MacKinnon, Polym. Degrad. Stab. 48 (1995) 341.
[9] J.H. Chan, S.T. Balke, Polym. Degrad. Stab. 57 (1997) 113.
[10] J.H. Chan, S.T. Balke, Polym. Degrad. Stab. 57 (1997) 135.
[11] C. Albano, E. de Freitas, Polym. Degrad. Stab. 61 (1998) 289.
[12] H. Bockhorn, A. Hornung, U. Hornung, D. Schawaller, J. Anal. Appl. Pyrol. 48 (1999) 93.
[13] B. Wielage, T. Lampke, G. Marx, K. Nestler, D. Starke, Thermochim. Acta 337 (1999) 169.
[14] J. Gersten, V. Fainberg, G. Hetsroni, Y. Shindler, Fuel 79 (2000) 1679.
[15] J. Yang, R. Miranda, C. Roy, Polym. Degrad. Stab. 73 (2001) 455.
[16] Z. Gao, T. Kaneko, I. Amasaki, M. Nakada, Polym. Degrad. Stab. 80 (2003) 269.
[17] R. Kumar, G. Madras, J. Polym. Sci. 90 (2003) 2206.
[18] J.D. Peterson, S. Vyazovkin, C.A. Wight, Macromol. Chem. Phys. 202 (2001) 775.
[19] D.N. Bikiaris, D.S. Achilias, D.J. Giliopoulos, G.P. Karayannidis, Eur. Polym. J. 42 (2006) 3190.
[20] D.N. Bikiaris, G.Z. Papageorgiou, E. Pavlidou, N. Vouroutzis, P. Palatzoglou, G.P. Karayannidis, J. Appl. Polym. Sci. 100 (2006) 2684.
[21] V. Vladimirov, C. Betchev, A. Vassiliou, G. Papageorgiou, D. Bikiaris, Comp. Sci. Techn. 66 (2006) 2935.
[22] Y. Liu, M. Kontopoulou, Polymer 47 (2006) 7731.
[23] D.N. Bikiaris, A. Vassiliou, E. Pavlidou, G.P. Karayannidis, Eur. Polym. J. 41 (2005) 1965.
[24] D.N. Bikiaris, V. Karavelidis, G.P. Karayannidis, Macromol. Rapid Commun. 27 (2006) 1199.
[25] S.C. Tjong, Mater. Sci. Eng. R 53 (2006) 73.
[26] S.S. Ray, M. Okamoto, Prog. Polym. Sci. 28 (2003) 1539.
[27] S.S. Ray, M. Bousmina, Prog. Mater. Sci. 50 (2005) 962.
[28] M. Alexandre, P. Dubois, Mater. Sci. Eng. R 28 (2000) 1.
[29] A.A. Vassiliou, G.Z. Papageorgiou, D.S. Achilias, D.N. Bikiaris, Macromol. Chem. Phys. 208 (2007) 364.
[30] K. Chrissafis, G. Antoniadis, K.M. Paraskevopoulos, A. Vassiliou, D.N. Bikiaris, Comp. Sci. Techn. 67 (2007) 2165.
[31] J.A. Lee, M. Kontopoulou, S.J. Parent, Macromol. Rapid. Commun. 28 (2007) 210.
[32] K. Chen, S. Vyazovkin, Macromol. Chem. Phys. 207 (2006) 587.
[33] J. Sun, T.D. Huang, G.T. Gong, H.L. Cao, Polym. Degrad. Stab. 91 (2006) 339.
[34] J. Macan, I. Brnardic, S. Orlic, H. Ivankovic, M. Ivankovic, Polym. Degrad. Stab. 91 (2006) 122.
[35] T. Ozawa, Bull. Chem. Soc. Japan 38 (1965) 188.
[36] J. Flynn, L.A. Wall, Polym. Lett. 4 (1966) 232.
[37] T. Ozawa, J. Therm. Anal. 2 (1970) 301.
[38] H.L. Friedman, J. Polym. Sci. C 6 (1964) 183.
[39] H.L. Friedman, J. Polym. Lett. 4 (1966) 323.
[40] S. Stavrev, U.S. Patent 5,353,708 (1994).
[41] D. Rivin, Rubber Chem. Tech. 44 (1971) 307.
[42] A. Vassiliou, D. Bikiaris, K. Chrissafis, K.M. Paraskevopoulos, S.Y. Stavrev, A. Docoslis, Thermochim. Acta 465 (2007) 6.
[43] Ch. Tselios, D. Bikiaris, P. Savidis, C. Panayioyou, J. Mater. Sci. 34 (1999) 385.

[44] A.S. Nielsen, R. Pyrz, Polym. Polym. Comp. 5 (1997) 245.
[45] J.S. Thomsen, R. Pyrz, Comp. Sci. Techn. 59 (1999) 1375.
[46] D. García-López, J.C. Merino, J.M. Pastor, J. Appl. Polym. Sci. 88 (2003) 947.
[47] W.J. Wang, Rubber Chem. Technol. 71 (1998) 520.
[48] S. Deng, L. Ye, K. Friedrich, J. Mater. Sci. 42 (2007) 2766.
[49] J.I. Velasco, M. Ardanuy, V. Realinho, M. Antunes, A.I. Fernández, J.I. González-Peña, M.A. Rodríguez-Pérez, J.A. de Saja, J. Appl. Polym. Sci. 102 (2006) 1213.
[50] H. Lu, X. Xu, X. Li, Z. Zhang, Bull. Mater. Sci. 29 (2006) 485.
[51] S.G. Lei, S.V. Hoa, M.T. Ton-That, Comp. Sci. Techn. 66 (2006) 1274.
[52] C.H. Lin, C.C. Feng, T.Y. Hwang, Eur. Polym. J. 43 (2007) 725.
[53] A.A. Arbash, Z. Ahmad, F. Al-Sagheer, A.A.M. Ali, J. Nanomater. (2006) 1–9.
[54] G.Z. Papageorgiou, D.S. Achilias, D.N. Bikiaris, G.P. Karayannidis, Thermochim. Acta 427 (2005) 117.
[55] M. Zanetti, G. Camino, R. Reichert, R. Mulhaupt, Macromol. Rapid Commun. 22 (2001) 176.
[56] Y. Tang, Y. Hu, L. Song, R. Zong, Z. Gui, Z. Chen, Polym. Degrad. Stab. 82 (2003) 127.
[57] H. Qin, S. Zhang, C. Zhao, M. Feng, M. Yang, Z. Shu, Polym. Degrad. Stab. 85 (2004) 807.
[58] K. Erdogan, J.K. Gillham, J. Appl. Polym. Sci. 20 (1976) 2045.
[59] R. Lattimer, J. Anal. Appl. Pyrol. 26 (1993) 65.
[60] S. Vyazovkin, J. Comput. Chem. 22 (2001) 178.
[61] S. Vyazovkin, Thermochim. Acta 355 (2000) 155.
[62] A. Burnham, Thermochim. Acta 355 (2000) 165.
[63] A. Jimenez, L. Torre, J.M. Kenny, Polym. Degrad. Stab. 73 (2001) 447.
[64] K. Chrissafis, K.M. Paraskevopoulos, D.N. Bikiaris, Polym. Degrad. Stab. 91 (2006) 60.
[65] K. Chrissafis, K.M. Paraskevopoulos, D.N. Bikiaris, Thermochim. Acta 440 (2006) 166.
[66] K. Chrissafis, K.M. Paraskevopoulos, D.N. Bikiaris, Thermochim. Acta 435 (2005) 142.
[67] S. Vyazovkin, C.A. Wight, Thermochim. Acta 340 (1999) 53.
[68] S. Vyazovkin, N. Sbirrazzuoli, Macromol. Rapid Commun. 27 (2006) 1515.